Reverberation Chamber Metrology for Wireless Internet of Things Devices

Anouk Hubrechsen, Kate A. Remley, and Sara Catteau

©SHUTTERSTOCK.COM/ZINETRON

Internet of things (IoT) devices are proliferating in our connected world, with the number of devices expected to exceed 14 billion in 2023 [1]. Wireless IoT applications are increasing day by day, ranging from cellular-enabled parking meters that can validate your credit card in real time, to trash compactors that inform the garbage company when they are full, to wireless local-area-network–enabled industrial programmable logic controllers (PLCs) that control robots on the factory floor with

Anouk Hubrechsen (a.hubrechsen@tue.nl) is with the Department of Electrical Engineering, Eindhoven University of Technology, Eindhoven, 5612 AZ, The Netherlands. Kate A. Remley (kate.remley@nist.gov) is with the National Institute of Standards and Technology, Boulder, Colorado, 80302, USA. Sara Catteau (sara.catteau@bluetest.se) is with Bluetest AB, 417 55, Gothenburg, Sweden.

Digital Object Identifier 10.1109/MMM.2021.3125464

Date of current version: 11 January 2022

One important strength related to the use of reverberation chambers for testing wireless devices is their flexibility in device placement and its form factor.

micron precision. The physical size and shape or *form factor* of these devices can range from millimeters to meters on a side, and latency requirements can range from hours (e.g., trash compactor) to seconds (e.g., parking meter) to milliseconds or less (e.g., factory floor sensing and control). With all of the possible variations, it is important to have flexible yet accurate test facilities for these devices.

Many wireless IoT devices have antennas integrated into the case or chassis, necessitating performance validation in an over-the-air (OTA) configuration [2], [3]. Besides that, some high-reliability applications, such as high-speed sensors and actuators operating on the factory floor, benefit from OTA testing in environmental conditions similar to those anticipated for deployment [4].

OTA testing of cellular-enabled IoT devices in anechoic chambers has been standardized for many years [3]. In these tests, a 3D characterization of the radiated performance of the device under test (DUT) is pieced together with data from spatially distributed measurements on a virtual sphere surrounding the DUT. Samples are typically spaced equidistantly along the θ and ϕ axes for each of two orthogonal polarizations. For example, in [3], the angular spacing was, at most, 15° for measurements of radiated power from the device, and 30° for measurements of the device's receiver sensitivity. Note that this approach may be sensitive to sampling errors and may be time intensive.

To overcome this, a reverberation chamber loaded with RF absorber may also be used instead of an anechoic chamber for OTA tests of wireless IoT devices. The reverberation chamber is an electrically large, reflective cavity that supports many modes. The fields corresponding to these modes add constructively and destructively at the receive antenna. As a result, the received power can vary significantly as a function of frequency and location of the receive antenna within the chamber. Fortunately, the modal structure can be significantly altered by changing the boundary conditions by moving metallic plates or paddles within the chamber. By averaging measurements made over a sufficient number and variety of static modal conditions (known as *stepped mode-stirring states*), power-based metrics such as total radiated power (TRP) and total isotropic sensitivity (TIS) can be estimated. Much recent research at the U.S. National Institute of Standards and Technology and other laboratories around the world has gone into quantifying the accuracy of such measurements [5]–[14], especially for cellular-enabled IoT devices. While outside of the scope of this work, reverberation chambers are also excellent candidates for characterization of antennas and channel capacities in diversity and multiple-input, multiple-output systems [7], [13], [15].

One important strength related to the use of reverberation chambers for testing wireless devices is their flexibility in device placement and its form factor. For example, placement of the device within the characterized *working volume* is not critical because the device's radiating element or elements will ideally be exposed to the same randomized fields anywhere in that volume. Parts of the device may even be outside of the working volume as long as they do not radiate (intentionally or unintentionally). Such flexibility is important for testing of physically large devices such as parking meters or vending machines because the exact location of the radiating elements may not be known and/or exact placement of the radiating element in a specified location of the working volume (as required for anechoic chamber measurements) may be challenging.

In this work, we provide an overview of how to perform reverberation-chamber wireless testing for IoT devices. We first provide a brief overview to introduce the main concepts in the use of reverberation chambers for OTA testing of wireless devices. We discuss reverberation-chamber-specific components of uncertainty in these types of measurements, such as the number of measured samples collected and the chamber configuration, including the efficiency measurement of the antennas. Our examples will focus on the characterization of low-cost cellular-enabled devices that use a spectrally efficient transmission protocol called narrowband IoT (NB-IoT) [16]. Because the antenna efficiency can be a complicated measurement for narrowband devices and it is an important contribution to other device performance metrics, we also discuss this. We then provide an example of an NB-IoT device measurement with corresponding uncertainties. These examples illustrate the flexibility that reverberation chambers can provide in terms of device placement within the chamber and the accuracy that can be achieved with relatively straightforward calibration procedures.

Reverberation Chamber Measurement Procedures

Averaging Is Key

To perform a measurement, the modal structure in the chamber is intentionally randomized by altering

the boundary conditions within the chamber or by probing the fields at different locations and/or polarizations within the chamber. The former is often accomplished by use of a mechanical mode-stirring paddle (as illustrated in Figure 1), while the latter is often accomplished by use of a rotating platform or by using multiple measurement antennas having different physical locations and polarizations. Measurement samples are averaged in postprocessing to obtain quantities such as TRP or TIS.

Because the quantities of interest must be derived by averaging, the uncertainty in the final estimate of that quantity will depend on the number of samples that were acquired. For measurements performed in an ideal, lossless reverberation chamber, the uncertainty due to the number of mode-stirring samples may be estimated as [17]

$$u = \frac{1}{\sqrt{MN}}, \tag{1}$$

where, generally, M and N represent various mode-stirring mechanisms. For example, M may be the number of antenna positions, and N the number of paddle positions. The above formula assumes that the environment is wide-sense stationary (that is, the mean and autocovariance are time invariant and that the expectation is finite for all times) and, consequently, that the measurement samples are independent and uncorrelated [18]. This assumption can be well satisfied in a high quality factor (high-Q) reverberation chamber whose configuration does not include much lossy RF absorbing material. Such unloaded chambers have been used for many years in continuous wave electromagnetic compatibility and electromagnetic interference testing.

However, such an environment is rarely appropriate for testing wireless devices that transmit digitally modulated communication signals. Communication signals may have instantaneous modulation bandwidths on the order of tens of kilohertz to tens of megahertz. For testing of these devices, such a high-Q environment may provide a *frequency selective* channel that can confuse the device's equalizers, which were designed to operate in real-world multipath environments that vary less as a function of frequency.

To provide an appropriate test environment for tests where we must demodulate the communication signal, we intentionally load the chamber with RF-absorbing material.

For tests that require demodulating a communication signal, these chamber-induced effects can make it appear that the DUT's performance is worse than it really would be under the real-world operating conditions for which it was designed. To provide an appropriate test environment for tests where we must demodulate the communication signal, we intentionally load the chamber with RF-absorbing material, leading to a host of issues that must be addressed for accurately characterizing the performance of the DUT. A few of these are summarized below, with more detail supplied in [12].

Chamber Loading and Coherence Bandwidth

Intentionally loading the chamber with RF absorber replicates the *flat-fading* channel conditions that wireless-device equalizers are designed to accommodate [6], [9], [12]. Figure 2 illustrates this, where we see that

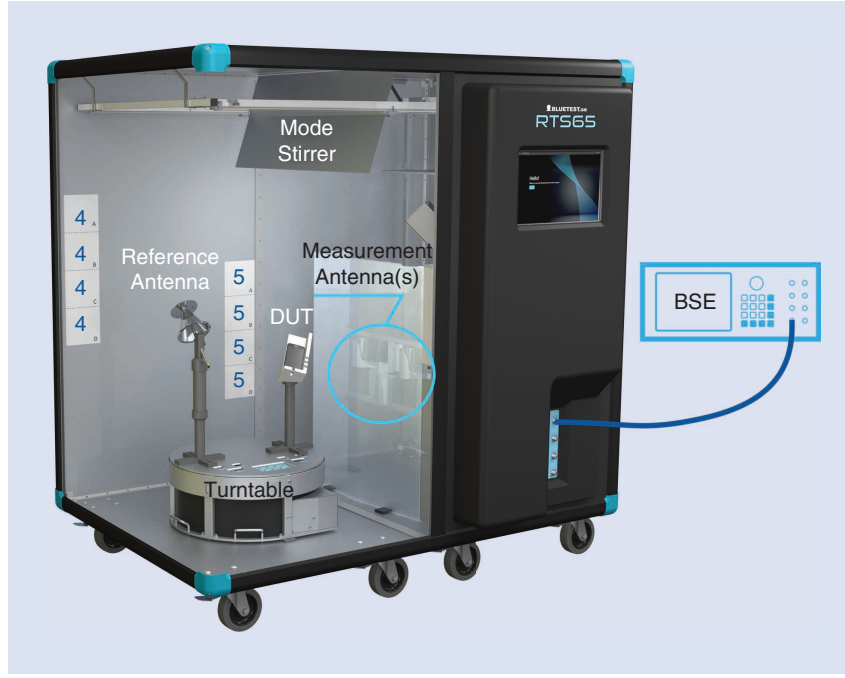

Figure 1. *A reverberation-chamber setup for TIS, including a turntable for position stirring, which is needed in loaded chamber measurements. The DUT is connected to a BSE, and it is disconnected for the reference measurement of G_{ref}, where both the reference and measurement antenna are connected to a VNA.*

a significant amount of absorbing material is needed to measure the correct value of receiver sensitivity, as indicated by the plateau in the value of TIS. As Figure 2 shows, once the channel is sufficiently flat, adding additional amounts of absorber does not significantly affect the mean value of the measured TIS, although the uncertainty due to lack of spatial uniformity may increase, as discussed in the "Uncertainties" section in the "Reverberation Chamber Measurement Procedures" section.

A common metric that allows us to assess the amount of frequency flattening provided by a given loading condition is the coherence bandwidth (CBW) [12]. The CBW was originally used in RF propagation channel modeling, describing the frequency separation

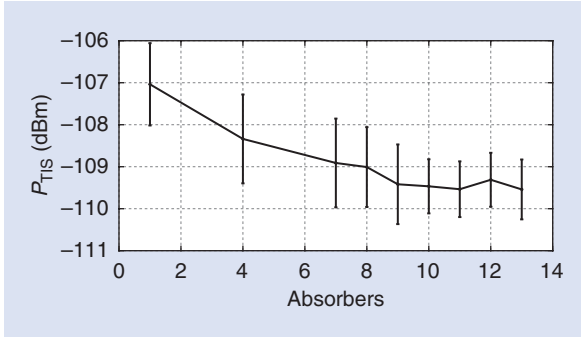

Figure 2. *Received power corresponding to the receiver's estimated TIS (P_{TIS}) as a function of chamber loading for a cellular device that transmits a wideband code division multiple access signal having a 3.84-MHz modulation bandwidth (from [9]). Error bars correspond to the standard uncertainty obtained from measurements made with nine independent realizations of the same stepped mode-stirring sequence in the chamber.*

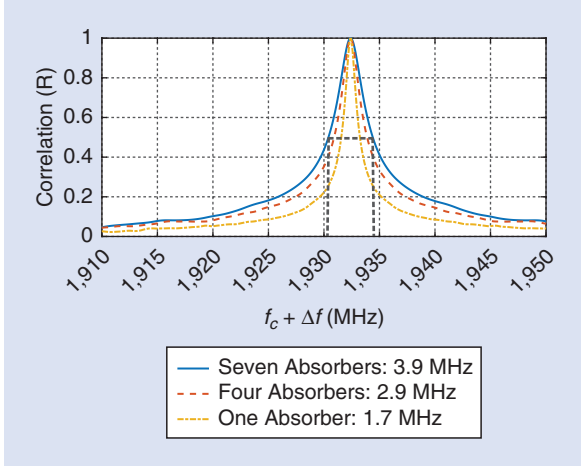

Figure 3. *The frequency autocorrelation function for a chamber loaded with three different amounts of RF absorber. The threshold of 0.5 is chosen here to define the CBW, as illustrated by the dotted gray lines (from [9]).*

necessary for two signals to be considered statistically independent [19]. A wider CBW corresponds to a smoother frequency response. The CBW has an inverse relationship to the quality factor of a reverberation chamber. That is, the more that a reverberation-chamber configuration stores energy, the more frequency selective the chamber setup is.

The CBW corresponding to a specific amount of loading can be estimated from the frequency autocorrelation of an S_{21} measurement as

$$R(i,n) = \frac{\sum_{j=1}^{P-i} S_{21}(f_j, n) S_{21}^*(f_{j+i}, n)}{\sum_{j=1}^{P-i} S_{21}(f_j, n) S_{21}^*(f_j, n)}, \quad (2)$$

where $S_{21}(f_j, n)$ corresponds to the measured complex S_{21} at frequency step f_j with P frequency points measured within the bandwidth of interest, BW, so that $f_1 = f_c - (BW/2)$ and $f_P = f_c + (BW/2)$. The index, n, is the mode-stirring sample (out of N). The index, i, corresponds to one of several frequency-step offsets (lags) over the BW (here $BW = 100$ MHz [2]), where $-(P-1) \le i \le (P-1)$. The frequency lag for a set of measured data will be given by $\Delta f = i(f_p - f_1/P - 1)$. The asterisk denotes complex conjugation. The BW is taken over 100 MHz to provide stable results, as has been previously shown in [12].

A representative set of CBW plots for loading with various amounts of RF absorber is shown in Figure 3, where we calculated the autocorrelation using (2). The CBW is computed for a defined threshold of the autocorrelation function. The width for a threshold of 0.5 is illustrated by the dotted line in Figure 3 for the seven-absorber case. In current practice (e.g., [2]), the CBW would be chosen to meet or exceed the modulation bandwidth of the communication signal being tested.

Spatial Uniformity

As mentioned in the previous section, a significant amount of loading may be needed for wireless device tests in order to accurately demodulate a communication signal. This loading increases the correlation between measured frequency samples to provide a flat-fading channel. On the downside, loading also increases spatial correlation between the sampled fields, whether at various positions of mechanical mode stirrers, between the locations of antennas, or even between antenna orientations. Such spatial correlation occurs because of an increase in unstirred energy relative to the stirred energy (a higher K-factor), which translates to an offset to the measured quantities. The issue with spatial correlation is that it reduces the number of

independent samples in the reverberation-chamber measurement, which can complicate the development of a stirring sequence that will provide sufficiently low uncertainty in the measurement of a quantity of interest. Understanding the lack of spatial uniformity is, therefore, crucial to understanding the accuracy of the measurement.

One method to assess the lack of spatial uniformity for a given chamber configuration considers the variation in measurements of multiple *independent realizations* of the stepped mode-stirring sequence (where independence can be evaluated by use of a cross-correlation procedure [2]). To explain what is meant by independent realizations, let us consider a 100-sample stirring sequence consisting of $N = 10$ different paddle angles and $M = 10$ different turntable locations. If the stirring sequence is well designed with uncorrelated samples, then any implementation of $M \times N = 100$ samples should provide the same result (within the specified working volume of the chamber and to within the desired uncertainty). Assuming an adequate number of samples is used [see (1)], any deviation from this result will correspond (approximately) to the lack of spatial uniformity in the chamber. For many wireless protocols, a lack of spatial uniformity dominates uncertainty in the measurement [10], [20]. However, for narrowband protocols, this is not always the case, as will be discussed in the next section.

Uncertainties

Many of the uncertainties in the estimate of metrics such as TRP or TIS from reverberation-chamber measurements are common to other OTA test techniques, such as anechoic or semi-anechoic chamber measurements. These include residual impedance mismatch, signal generator stability, temperature effects, and repeatability [10]. However, there are a number of components of uncertainty that are specific to reverberation-chamber measurements of wireless devices. These include the number of samples *within* a mode-stirring sequence [17] and the uncertainty due to the lack of spatial uniformity *between* stirring sequences just mentioned. These two components of uncertainty may be difficult to characterize individually because one parameter (e.g., number of mode-stirring samples) can affect the other (e.g., impact of lack of spatial uniformity).

Thus, for a given chamber setup and modulated signal bandwidth, it is common to perform a significance test to determine whether an uncertainty formulation should be used that assumes that both the *within* and the between uncertainty are significant or a formulation that assumes only the *between* uncertainty is significant [20]. A method for calculating these components of uncertainty is presented in the next section.

Generally, for testing wireless devices in loaded reverberation chambers, the uncertainty due to the chamber configuration's lack of spatial uniformity dominates.

Generally, for testing wireless devices in loaded reverberation chambers, the uncertainty due to the chamber configuration's lack of spatial uniformity dominates. As mentioned previously, this type of uncertainty is generally estimated from the difference in measurements of the chamber's transfer function [i.e., the chamber loss (G_{ref})] between independent realizations (we usually use a minimum of nine independent realizations [2], [12]). However, for narrowband transmission formats such as NB-IoT, the uncertainty due to differences within the independent realizations may become significant, as shown in [10]. If this is the case, a different formulation should be used for uncertainty, yielding a lower uncertainty estimate than the formulation that assumes only between uncertainty to be significant.

Another component of uncertainty that plays a role in reverberation chamber measurements is the uncertainty in the estimate of measurement antenna efficiency. Reverberation-chamber calibrations require an estimate of the efficiency of the measurement antenna, in contrast to most anechoic chamber measurements, which focus on antenna gain rather than efficiency. An estimation of antenna efficiency can be carried out from reverberation-chamber measurements [21]–[27]. This is a separate step from the DUT and chamber characterization measurements, and some of the issues related to this are described in the section "Antenna Efficiency."

To estimate the expanded uncertainty in the DUT measurement, other contributions should be taken into account as well, according to the cellular industry association CTIA test plan [2], [3] (e.g., uncertainty in the antenna mismatch, the base-station emulator (BSE) output level stability, the sensitivity in the search step size, the temperature variation, frequency resolution and miscellaneous uncertainty). The total expanded uncertainty of the full TRP or TIS measurement is estimated by taking the root-sum-square of the uncertainty in both the reference and the DUT measurements [2]. Note that the total expanded uncertainty should be below 2 dB for TRP to comply to the CTIA test plan. Because TIS measurements are performed near the noise floor of the DUT's receiver, this limit is expanded to 2.3 dB for TIS.

IoT Device Measurements

Metrics

Two main metrics of interest for wireless device measurements are TRP and TIS. To accurately characterize them, two measurements must be performed: a chamber characterization *Reference* measurement using a vector network analyzer (VNA) and the measurement of the DUT itself, using a BSE, as illustrated in Figure 1. All measurement procedures described are according to the standardized CTIA test methods [2].

TRP is a measure of the total power radiated by the DUT in all directions. When measuring TRP, the BSE is configured to request the maximum radiated power from the DUT. Next, the average received power across the channel is measured at the BSE with an integrated spectrum analyzer. This process is repeated for each mode-stirring state and corrected for the chamber, cable, and antenna loss, where TRP is calculated as

$$P_{\text{TRP}} = \frac{\langle \langle P_R^n \rangle_N \rangle_F}{G_{\text{ref}} \eta_{\text{meas}}^{\text{tot}} G_{\text{cable}}}, \tag{3}$$

where P_R^n is the received power for a mode-stirring sample n; $\langle \cdot \rangle_N$ is the ensemble average over N mode-stirring samples; F is the bandwidth over which the samples are frequency averaged, where the received power is averaged over the channel bandwidth; G_{ref} and G_{cable} are the chamber and cable loss, respectively; and $\eta_{\text{meas}}^{\text{tot}}$ is the total efficiency of the measurement antenna (illustrated in Figure 1 behind the semitransparent blocking plate). The latter three variables are extracted from two separate reference measurements.

TIS is a measure of the minimum received power accepted by a device without incurring an unacceptably low or high bit error rate, respectively. To measure TIS for NB-IoT, the BSE sets up a connection with the DUT and measures the throughput for various input powers. According to the CTIA test plan [2], TIS for NB-IoT corresponds to the minimum downlink power required to provide a data throughput rate greater than or equal to 95% of the maximum throughput of the reference measurement channel. The input power of the BSE is stepped down until the BSE reaches the throughput threshold. This process is repeated for all stirring positions and, similar to TRP measurement, also corrected for the cable, chamber, and antenna losses, where TIS is calculated using

$$P_{\text{TIS}} = G_{\text{ref}} \eta_{\text{meas}}^{\text{tot}} G_{\text{cable}} \left(\left\langle \frac{1}{P_{\text{BSE}}^n} \right\rangle_N \right)^{-1}, \tag{4}$$

where P_{TIS} is the TIS in watt, and P_{BSE} is the input power provided by the BSE.

Reference Measurement

The reference measurement is performed to estimate the G_{ref} (including loading). The setup used is the same as in Figure 1, but a reference antenna is used instead of the DUT (as shown in Figure 1). The reference and measurement antennas are connected to a VNA instead of a BSE. The DUT and the fixture that holds it are present in the chamber to maintain the same loading, but the DUT is powered off. Using an S_{21} measurement, the G_{ref} can be calculated using

$$G_{\text{ref}} = \frac{\langle \langle |S_{21}|^2 \rangle_N \rangle_F}{\eta_{\text{meas}}^{\text{tot}} \eta_{\text{ref}}^{\text{tot}}}, \tag{5}$$

where $\eta_{\text{ref}}^{\text{tot}}$ is the total efficiency of a separate reference antenna that is not included in the DUT measurement. Generally, the antenna will be integrated into the NB-IoT device, so this cannot be used as a reference antenna. To accurately represent the situation in the chamber during the DUT measurement, a reference antenna should be used that has a similar radiation pattern as the one on the device. Such antennas may have a high frequency selectivity or high rejection band, which makes it more challenging to measure them in a reverberation chamber, as we will show in the "Antenna Efficiency" section.

The uncertainty due to lack of spatial uniformity, discussed in the previous section, can be extracted from the standard deviation in G_{ref} between N_B independent realizations given by

$$\sigma_{G_{\text{ref}}} = \sqrt{\frac{1}{N_B - 1} \sum_{b=1}^{N_B} (\langle G_{\text{ref},b} \rangle_{N_W} - \hat{G}_{\text{ref}})}, \tag{6}$$

where $\langle G_{\text{ref},b} \rangle_{N_W}$ is the chamber transfer function for a given independent realization b, averaged over all N_W mode-stirring samples within b, and where $\hat{G}_{\text{ref}}$ is the mean of all N_B independent realizations. This formulation assumes only the differences between independent realizations to be statistically significant, as used in the current test plan [2]. The uncertainty due to lack of spatial uniformity for the reference measurement is then given by

$$u_{\text{ref},B} = \sqrt{\frac{1}{N_B} \sigma_{G_{\text{ref}}}^2}. \tag{7}$$

When the uncertainty within independent realizations is also statistically significant (as discussed in [20]), the uncertainty for the reference measurement is given by

$$u_{\text{ref}} = \sqrt{\frac{1}{N_B N_W (N_B N_W - 1)} \sum_{b=1}^{N_B} \sum_{w=1}^{N_W} (G_{\text{ref},b,w} - \hat{G}_{\text{ref}})}. \tag{8}$$

Depending on the chamber configuration and the mode-stirring sequence, this formulation may need to be used, as was shown in [10]. Note that this formulation tends to yield a lower uncertainty, but that, for ease of implementation, the current CTIA test plan assumes that only the between uncertainty is statistically significant [2].

DUT Measurement

For the DUT measurement, only the DUT and the measurement antenna are used, where the latter is connected to a BSE. The DUT is connected only to a power source and not to the BSE directly. The reference antenna is not used in this measurement but, rather, remains in the chamber and is terminated in a 50-Ω load, again to maintain the same chamber loading for both the Reference and DUT measurements. For the DUT measurement, a lab typically performs only a single measurement (or independent realization) to reduce measurement time. In that case, $u^2_{\mathrm{DUT}} = \sigma^2_{G_{\mathrm{ref}}}$. Therefore, the uncertainty in the DUT measurement is often higher than the reference measurement. For example, in the setup used in [10], we showed that, for the NB-IoT protocol, both between and within independent-realization differences were statistically significant, where the uncertainty was 0.42 dB for the DUT measurement, but only 0.18 dB for the reference measurement. In the "NB-IoT Device Measurement Results" section, we will show results of TRP and TIS measurements of different cellular and NB-IoT devices, including the calculation of uncertainty.

Antenna Efficiency

As can be seen in (3) and (4), antenna efficiency plays an important role in determining the TRP and TIS of wireless devices. A variety of methods exist to estimate antenna efficiency in a reverberation chamber [21]–[27]. To estimate antenna efficiency, a separate measurement of the reference power transfer function should be performed in an unloaded (or very lightly loaded) chamber since RF absorbers can act as an additional antenna load which may yield an incorrect estimate or high uncertainty, as was shown in [28]. Therefore, the antenna efficiency is generally not derived from the TRP/TIS-loaded reference measurements described in the "Reference Measurement" section of the "IoT Device Measurements" section but, rather, from a second unloaded reference measurement. In this section, we describe several of the most common methods for deriving antenna efficiency from reverberation-chamber measurements, along with their advantages and constraints. We refer to the total antenna efficiency as the ratio of the radiated power and the power arriving at the antenna port and the radiated antenna efficiency as the power accepted by the port. Reverberation-chamber measurement methods generally estimate the total antenna efficiency, from which the radiation efficiency may be derived by correcting for the mismatch at the antenna port.

In Figure 4, we show results for the total antenna efficiency of an antenna that could be used in future IoT applications, originally presented in [29], computed using different methods. This antenna is frequency reconfigurable, and we tuned it to have a narrow operating band centered at 1.4 GHz. It is important to note that this antenna has a high rejection band adjacent to the operating band, which caused the large discrepancies between estimates calculated with different methods. In this case, the dashed black and dotted blue curves in Figure 4 provide the correct estimate, while the solid-yellow curves and the dash-dotted red curves show an overestimated approximation, as we will discuss.

When an antenna replacement method (using three antennas) is used to assess antenna efficiency, one antenna with a known efficiency is required to be used as a reference antenna.

We extracted all data from a single measurement, where the IoT antenna and two dual-ridge horn antennas were present in an unloaded reverberation chamber. All three were connected to a VNA. We measured 12 positions with 100 stepped mode-stirring samples each, from which we extracted the uncertainty due to differences between independent realizations. The error bars in Figure 4 correspond to the uncertainty due to differences between independent realizations from (7), where each independent realization corresponds to a different antenna position. We refer the reader to Use Case 1 as presented in [30] for a more extensive explanation of the setup used.

According to the International Electrotechnical Commission (IEC) standard [27], when an antenna replacement method (using three antennas) is used to assess antenna efficiency, one antenna with a known

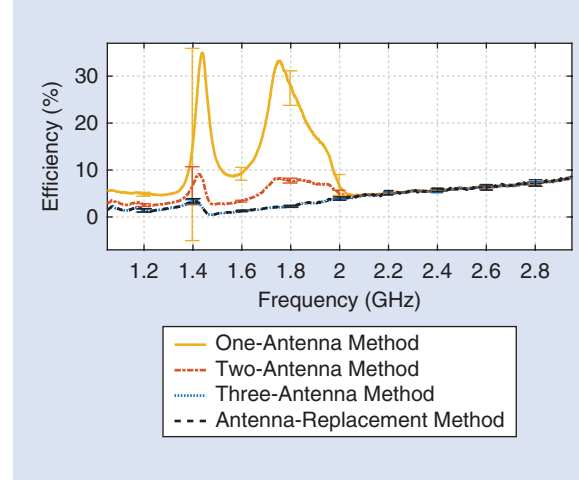

Figure 4. *A comparison of the efficiency estimate of an IoT antenna presented in [29], estimated with four different methods.*

efficiency is required to be used as a reference antenna. A second antenna may be any other antenna whose operational band is within the band of interest. The transmission coefficient between the two is measured as a reference, $S_{21,\mathrm{Ref}}$. Then, the reference antenna is replaced with the antenna under test (AUT), and the transmission coefficient between the two, $S_{21,\mathrm{AUT}}$, is measured. The total efficiency of the AUT can then be calculated as

$$\eta_{\mathrm{AUT}}^{\mathrm{tot}} = \frac{\langle\langle |S_{21,\mathrm{AUT}}|^2\rangle_N\rangle_F}{\langle\langle |S_{21,\mathrm{Ref}}|^2\rangle_N\rangle_F}\eta_{\mathrm{Ref}}^{\mathrm{tot}}, \tag{9}$$

where $\eta_{\mathrm{Ref}}^{\mathrm{tot}}$ is the total efficiency of the reference antenna. The result of the IoT antenna computed with this method is shown in Figure 4, where we used a dual-ridge horn antenna as a reference antenna. The efficiency of the reference antenna was extracted from the nonreference three-antenna method described below.

The antenna replacement method assumes that the G_{ref} does not change significantly when the reference antenna is replaced with the AUT. In reality, this may not be the case, as any discrepancy will lead to an over- or underestimation of the AUT's efficiency. Another challenge of this method is that an antenna with a known efficiency is required. To overcome this, nonreference antenna methods have been developed and are described next.

A few of the most common nonreference antenna methods are Holloway's reverberation chamber-based one-, two-, and three-antenna methods, presented in [25]. They are based on the assumption that the chamber's Q, as computed in the time domain (Q_{TD}), does not contain the losses due to the antennas' efficiencies (because the early- and late-time behavior are removed), while the Q computed in the frequency domain (Q_{FD}) does (both of these metrics can be extracted from an S_{21} measurement). Therefore, the efficiencies can be extracted by dividing the two as

$$\eta_1^{\mathrm{tot}}\eta_2^{\mathrm{tot}} = \frac{Q_{\mathrm{FD}}}{Q_{\mathrm{TD}}}, \tag{10}$$

where $Q_{\mathrm{FD}} = 16\pi^2 V\langle |S_{21}|^2\rangle/\lambda^3$, with V the chamber volume and λ the wavelength. $Q_{\mathrm{TD}} = 2\pi f\tau_{\mathrm{RC}}$, where τ_{RC} is the chamber decay time, defined by the exponentially decaying part of the S_{21} time domain response.

Equation (10) has three unknowns, so the equation can be solved when the transmission coefficient is measured between all combinations of three antennas. This is the concept behind the three-antenna method, which yields three equations [25]. The result of this method is shown by the dotted blue line in Figure 4, where the estimate has a low uncertainty and is within the uncertainty bounds of the antenna-replacement method.

Equation (10) can also be solved by measuring only two, or even only one, antenna with some additional assumptions. The two-antenna method assumes that the ratio between the reflection and the transmission coefficients, the so-called enhanced backscattering constant (e_b), to be constant for every antenna position, polarization, and orientation in the chamber. Therefore, the two-antenna method not only relies on transmission coefficients but also on reflection coefficients. One property of these methods is that e_b is not always constant over position [31]. Another is that noise can introduce a large systematic error in combination with a high uncertainty in the measured estimate, even while the signal-to-noise ratio of the total S-parameter remains high [26], [30]. This is due to the fact that, in some situations, randomly distributed samples of the paddles cannot be distinguished from random noise. Owing to the high rejection band of this antenna, one component of the measured reflection coefficient, S_{11}, the so-called stirred-energy component, is dominated by the measurement noise rather than by the fields that have been randomized by the mode-stirring mechanisms. This component is, therefore, overestimated, resulting in a direct overestimation of the antenna efficiency. As shown by the dot-dashed red curve in Figure 4, this systematic error can vary significantly over frequency.

The one-antenna method relies on the measurement of reflection coefficients by assuming that $e_b = 2$. This makes it even more susceptible to noise, as shown by the solid-yellow curve in Figure 4. Note that this is especially problematic for IoT devices with a narrow operating band, or a high rejection band, such as the one used in this work, where a significant overestimation of efficiency occurred. For this reason among others, it is typical to use the antenna replacement method for certification tests, or the three-antenna nonreference antenna method when no antenna with a known efficiency is available.

NB-IoT Device Measurement Results

To illustrate the use of the reverberation chamber for measuring IoT devices, we compare measurements of a standard cellular handset to measurements of an NB-IoT device. Our NB-IoT device was a development board that operates over several frequency bands and intended for use by the designers of IoT equipment. We illustrate measurements made for these devices using protocols that have similar frequency bandwidths: Global System for Mobile (GSM), with a 200-kHz channel size, and NB-IoT, with a 180-kHz channel size. Because these two bandwidths are comparable, this more or less eliminates the bandwidth dependence in

the results that we show. Because frequency averaging can significantly lower the uncertainty in the estimate of TRP or TIS, the uncertainties for these transmission protocols are typically higher than what might be obtained for a transmission protocol having a wider modulation bandwidth.

As discussed in the "IoT Device Measurements" section, TIS is measured by acquiring the value of the base station output power for which the DUT exceeds a specified error threshold measured over increasingly low output power levels. For the GSM protocol, the error threshold is defined by a 2.44% bit error rate [3]. For the NB-IoT protocol, the error threshold is defined as less than 95% of the maximum data throughput [3]. Other protocols use different thresholds, generally depending on the expected reliability of the specific air link.

We will first show measurements of three different cellular handsets in one specific band to illustrate the typical level of device variation and measurement reproducibility that can be expected for these types of measurements. For this first set of measurements, we intentionally used the lower range of the sub-6-GHz cellular spectrum (GSM Band 5 Channel 190, with a center frequency of approximately 881.6 MHz). Because reverberation chambers support fewer modes at lower frequencies, these bands tend to be more difficult to measure in terms of uncertainty. In our second set of measurements, we measured TIS for the NB-IoT device in a lower and higher frequency band (NB-IoT B28 Channel 9435, with a center frequency of approximately 789.5 MHz, and NB-IoT B1 Channel 300, with a center frequency of 2,140 MHz). These measurements are intended to illustrate the expected improvement in measurement uncertainty for the higher band.

All measurements were performed in the reverberation chamber illustrated in Figure 1. The chamber was loaded such that the CBW exceeded the channel bandwidth of the protocol to be tested. Extra loading ensured that the peaks of the narrowband signals did not drive the receivers in either the DUT or the BSE into a nonlinear operating state.

Two hundred stepped mode-stirring samples were acquired for each measurement and TIS was calculated using (4). Table 1 shows the results. The three GSM phone measurements agreed to within 1 dB. As previously mentioned, the CTIA requires a total measurement uncertainty for TIS of less than 2.3 dB, so nominal agreement is seen for these devices. The uncertainty due to lack of spatial uniformity ($\sigma_{G_{\text{ref}}}$) is presented for all three devices in Figure 5. This metric is plotted rather than (7) because it reflects the contribution to uncertainty of the nonideal chamber performance prior to combination with other components of uncertainty. Figure 5 shows that for increasingly wide frequency averaging bandwidths, the $\sigma_{G_{\text{ref}}}$ estimate decreases. Since the averaging bandwidth is generally chosen to be the same as the channel bandwidth, this uncertainty tends to be higher for narrowband devices, illustrating one of the key challenges of testing these devices. Note that the reduced frequency range for higher averaging bandwidths occurs due to the running-average technique used.

The TIS from the NB-IoT device is not directly comparable to that of the cellular handset because of the different error-threshold metric used [bit error rate (BER) versus throughput]. Nonetheless, the expanded measurement uncertainty for these measurements is below the CTIA threshold. Our purpose here is primarily to illustrate the method and provide some typical results.

Concluding Thoughts, Developments, and Trends

A reverberation chamber is an excellent candidate to perform fast (on the order of minutes), accurate, and flexible measurements of wideband and narrowband, single-input, single-output devices used for IoT applications, as we have shown. While the uncertainty may increase for narrowband protocols owing to a lower frequency averaging bandwidth as compared with earlier-generation protocols, we have shown that the deviation in measured TIS still adheres to the current standardized test methods [2], [3].

However, with the reduction in production costs, the test time needs to be reduced as well. One way to achieve a reduced test time is by adjusting the type of mode stirring. Current standardized reverberation-chamber

TABLE 1. TIS results, measurement settings, and uncertainty for different devices for GSM and NB-IoT.

Device	Band	Channel	Center Frequency	BW (kHz)	CBW (MHz)	TIS (dB)	Threshold	$\sigma_{G_{\text{Ref}}}$ (dB)
Cell Phone 1	B5	190	881.6 MHz	200	5.5543	–103.3	2.44% BER	0.6
Cell Phone 2	B5	190	881.6 MHz	200	5.5543	–102.8	2.44% BER	0.6
Cell Phone 3	B5	190	881.6 MHz	200	5.5543	–102.5	2.44% BER	0.6
NB-IoT Device	B1	300	2,140 MHz	180	2.5768	–123.1	95% Throughput	0.5
NB-IoT Device	B28	9435	789.5 MHz	180	4.9195	–119.2	95% Throughput	0.4

measurement methods are based on stepped-mode stirring, where measurement samples are collected in a series of static channels. Because of the huge number of new, often low-cost, IoT devices, increasing the speed for these tests is of great interest in the wireless telecommunications industry. New methods based on continuous stirring in reverberation chambers are being explored. Such test methods may be appropriate for cases where uncertainties can be relaxed, that is, for cases where it is desired to produce a reasonably accurate result in as little time as possible. One example is for the testing of inexpensive, cellular-enabled IoT devices.

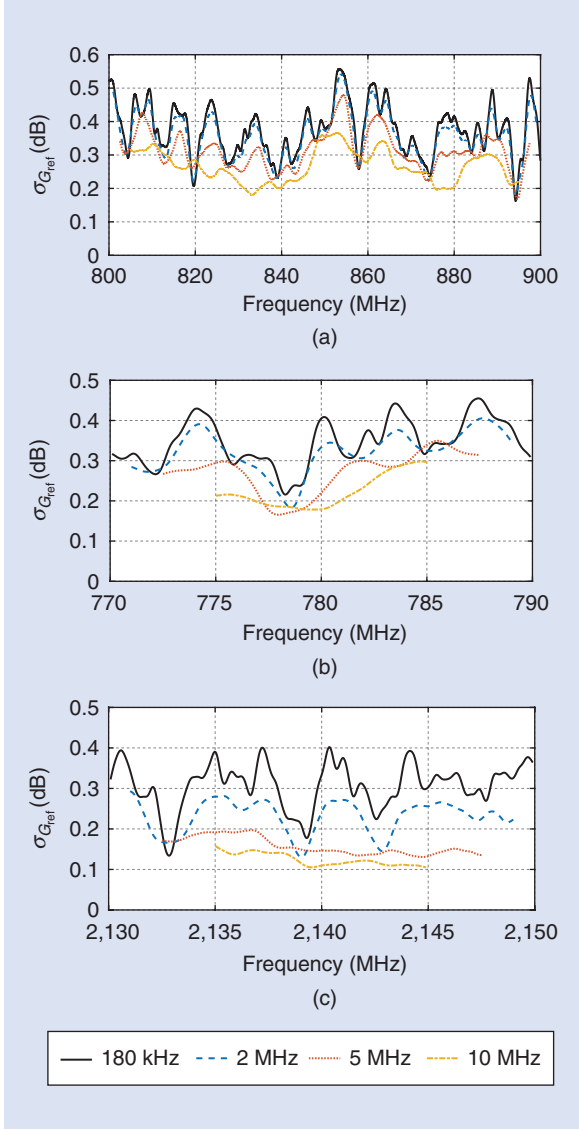

Figure 5. *The $\sigma_{G_{ref}}$ computed with various averaging bandwidths. (a) A setup with a cellular handset for GSM (CBW = 5.5543 MHz). Setups with an NB-IoT device for a center frequency of (b) 780 MHz (CBW = 2.5758 MHz), and (c) 2,140 MHz (CBW = 4.9195 MHz).*

A second example where continuous stirring may be beneficial is for the testing of intermediate channels in cellular devices. For intermediate-channel testing, full TIS measurements are performed at the low-, mid-, and high-channels of a given cellular band. Rapid testing at intermediate-channel frequencies provides a quick indication of the device's radiated performance to ensure there is no serious frequency selective behavior (e.g., an antenna "suck-out") due to unintended resonances in the integrated device. Methods are under development, such as that proposed in [32].

Another forward-looking application involves the creation of *spatial channels* that correspond to specific propagation-channel conditions. Current certification tests such as the ones described here, focus on power-based metrics such as TRP and TIS in isotropic conditions, similar to those provided by an anechoic chamber. By replicating realistic channel conditions, such as those found in outdoor urban environments [7] or on the factory floor [33], wireless devices with multiple and/or active antennas may be tested more comprehensively.

Reverberation-chamber research is underway at millimeter-wave frequencies as well [34]–[37], which is important as wireless devices start to operate in higher and higher bands. In summary, wireless technology is increasingly prevalent in many different applications that use a wide range of form factors and transmission protocols. The flexibility and accuracy provided by reverberation chambers—when properly configured and characterized—will likely play an increasingly important role in OTA testing.

Acknowledgments

The authors thank the reviewers, Sander Bronckers and Robert Horansky for their thorough reviews of this manuscript, as well as Robert Jones, Carnot Nogueira, and Vincent Neylon for their technical support.

References

[1] "Cisco annual internet report (2018–2023) white paper," Cisco, San Francisco, CA, USA, Tech. Rep., Mar. 2020. [Online] Available: https://www.cisco.com/c/en/us/solutions/collateral/executive-perspectives/annual-internet-report/white-paper-c11-741490.html

[2] "Test plan for wireless large-form-factor device over-the-air performance," CTIA Certification, Washington, DC, USA, Version 1.2.1, Feb. 2019. [Online]. Available: https://api.ctia.org/wp-content/uploads/2019/02/CTIA-Test-Plan-for-Wireless-Large-Form-Factor-Device-Over-the-Air-Performance-Version-1.2.pdf

[3] "Test plan for wireless over-the-air performance: Method of measurement for radiated RF power and receiver performance," CTIA Certification, Washington, DC, USA, Version 3.9, Nov. 2019. [Online]. Available: https://api.ctia.org/wp-content/uploads/2019/04/CTIA_OTA_Test_Plan_3_8_2.pdf

[4] R. Candell and M. Kashef, "Industrial wireless: Problem space, success considerations, technologies, and future direction," in *Proc.*

Int. Symp. Resilient Commun. Syst., Wilmington, DE, USA, Sep. 22, 2017, pp. 133–139, doi: 10.1109/RWEEK.2017.8088661.

[5] C. Orlenius, P. Kildal, and G. Poilasne, "Measurements of total isotropic sensitivity and average fading sensitivity of CDMA phones in reverberation chamber," in *Proc. 2005 IEEE Antennas Propag. Soc. Int. Symp.*, vol. 1A, pp. 409–412, doi: 10.1109/APS.2005.1551339.

[6] X. Chen *et al.*, "Reverberation chambers for over-the-air tests: An overview of two decades of research," *IEEE Access*, vol. 6, pp. 49,129–49,143, Aug. 2018, doi: 10.1109/ACCESS.2018.2867228.

[7] P. Kildal, C. Orlenius, and J. Carlsson, "OTA testing in multipath of antennas and wireless devices with MIMO and OFDM," *Proc. IEEE*, vol. 100, no. 7, pp. 2145–2157, 2012, doi: 10.1109/JPROC.2012.2188129.

[8] O. Delangre, P. De Doncker, F. Horlin, M. Lienard, and P. Degauque, "Reverberation chamber environment for testing communication systems: Applications to OFDM and SC-FDE," in *Proc. 2008 IEEE 68th Veh. Technol. Conf.*, pp. 1–5, doi: 10.1109/VETECF.2008.56.

[9] R. D. Horansky and K. A. Remley, "Flexibility in over-the-air testing of receiver sensitivity with reverberation chambers," *IET Microw., Antennas Propag.*, vol. 13, no. 15, pp. 2590–2597, 2019, doi: 10.1049/iet-map.2019.0417.

[10] A. Hubrechsen, K. A. Remley, R. D. Jones, R. D. Horansky, V. T. Neylon, and L. A. Bronckers, "NB-IoT devices in reverberation chambers: A comprehensive uncertainty analysis," *Int. J. Microw. Wireless Technol.*, vol. 13, no. 6, pp. 1–8, 2021, doi: 10.1017/S1759078721000192.

[11] J. Luo, E. Mendivil, and M. Christopher, "Over-the-air performance evaluation of NB-IoT in reverberation chamber and anechoic chamber," in *Proc. AMTA*, Nov. 2018, pp. 1–3.

[12] K. A. Remley *et al.*, "Configuring and verifying reverberation chambers for testing cellular wireless devices," *IEEE Trans. Electromagn. Compat.*, vol. 58, no. 3, pp. 661–672, Jun. 2016, doi: 10.1109/TEMC.2016.2549031.

[13] P.-S. Kildal, X. Chen, C. Orlenius, M. Franzen, and C. S. L. Patane, "Characterization of reverberation chambers for OTA measurements of wireless devices: Physical formulations of channel matrix and new uncertainty formula," *IEEE Trans. Antennas Propag.*, vol. 60, no. 8, pp. 3875–3891, 2012, doi: 10.1109/TAP.2012.2201125.

[14] Q. Xu *et al.*, "Measuring the total radiated power of wideband signals in a reverberation chamber," *IEEE Antennas Wireless Propag. Lett.*, vol. 19, no. 12, pp. 2260–2264, 2020, doi: 10.1109/LAWP.2020.3029793.

[15] P.-S. Kildal and K. Rosengren, "Correlation and capacity of MIMO systems and mutual coupling, radiation efficiency, and diversity gain of their antennas: Simulations and measurements in a reverberation chamber," *IEEE Commun. Mag.*, vol. 42, no. 12, pp. 104–112, 2004, doi: 10.1109/MCOM.2004.1367562.

[16] "User equipment (UE) radio transmission and reception; part 1: Range 1 standalone (Release 16)," 3GPP, Sophia Antipolis, Tech. Specification 38.101-1: NR, Sep. 2020.

[17] J. G. Kostas and B. Boverie, "Statistical model for a mode-stirred chamber," *IEEE Trans. Electromagn. Compat.*, vol. 33, no. 4, pp. 366–370, 1991, doi: 10.1109/15.99120.

[18] R. J. Pirkl, K. A. Remley, and C. S. L. Patane, "Reverberation chamber measurement correlation," *IEEE Trans. Electromagn. Compat.*, vol. 54, no. 3, pp. 533–545, 2012, doi: 10.1109/TEMC.2011.2166964.

[19] W. C. Jakes, "Multipath interference," in *Microwave Mobile Communications*. New York, NY, USA: IEEE Press, 1974.

[20] K. A. Remley, C.-M. J. Wang, D. F. Williams, J. J. Aan den Toorn, and C. L. Holloway, "A significance test for reverberation-chamber measurement uncertainty in total radiated power of wireless devices," *IEEE Trans. Electromagn. Compat.*, vol. 58, no. 1, pp. 207–219, Feb. 2016, doi: 10.1109/TEMC.2015.2481891.

[21] C. S. Lee, A. Duffy, and C. Lee, "Antenna efficiency measurements in a reverberation chamber without the need for a reference antenna," *IEEE Antennas Wireless Propag. Lett.*, vol. 7, pp. 448–450, Feb. 2008, doi: 10.1109/LAWP.2008.2002262.

[22] A. Khaleghi, "Time-domain measurement of antenna efficiency in reverberation chamber," *IEEE Trans. Antennas Propag.*, vol. 57, no. 3, pp. 817–821, Mar. 2009, doi: 10.1109/TAP.2009.2013445.

[23] H. G. Krauthäuser and M. Herbrig, "Yet another antenna efficiency measurement method in reverberation chambers," in *Proc. IEEE Int. Symp. Electromagn. Compat.*, Jul. 2010, pp. 536–540, doi: 10.1109/ISEMC.2010.5711333.

[24] A. Gifuni, I. D. Flintoft, S. J. Bale, G. C. R. Melia, and A. C. Marvin, "A theory of alternative methods for measurements of absorption cross section and antenna radiation efficiency using nested and contiguous reverberation chambers," *IEEE Trans. Electromagn. Compat.*, vol. 58, no. 3, pp. 678–685, Jun. 2016, doi: 10.1109/TEMC.2016.2548939.

[25] C. L. Holloway, H. A. Shah, R. J. Pirkl, W. F. Young, D. A. Hill, and J. Ladbury, "Reverberation chamber techniques for determining the radiation and total efficiency of antennas," *IEEE Trans. Antennas Propag.*, vol. 60, no. 4, pp. 1758–1770, Apr. 2012, doi: 10.1109/TAP.2012.2186263.

[26] Q. Xu, Y. Huang, X. Zhu, L. Xing, Z. Tian, and C. Song, "A modified two-antenna method to measure the radiation efficiency of antennas in a reverberation chamber," *IEEE Antennas Wireless Propag. Lett.*, vol. 15, pp. 336–339, Jun. 2015, doi: 10.1109/LAWP.2015.2443987.

[27] "Electromagnetic compatibility (EMC) part 4: Testing and measurement techniques; section 21: Reverberation chamber test methods," International Electrotechnical Commission, Geneva, Switzerland, Tech. Rep. IEC 61000-4-21, 2001.

[28] W. T. C. Burger, C. L. Holloway, and K. A. Remley, "Proximity and orientation influence on q-factor with respect to large-form-factor loads in a reverberation chamber," in *Proc. 2013 Int. Symp. Electromagn. Compat.*, pp. 369–374, doi: 10.1109/ISEMC.2013.6670496.

[29] L. A. Bronckers, A. Roc'h, and A. B. Smolders, "A new design method for frequency- reconfigurable antennas using multiple tuning components," *IEEE Trans. Antennas Propag.*, vol. 67, no. 12, pp. 7285–7295, Dec. 2019, doi: 10.1109/TAP.2019.2930204.

[30] A. Hubrechsen *et al.*, "The effect of noise on reverberation-chamber measurements of antenna efficiency," *IEEE Trans. Antennas Propag.*, early access, doi: 10.1109/TAP.2021.3083822.

[31] L. A. Bronckers, A. Roc'h, and A. B. Smolders, "Reverberation chamber enhanced backscattering: High-frequency effects," in *Proc. Int. Symp. Electromagn. Compat. EMC EUROPE*, Sep. 2019, pp. 1–6, doi: 10.1109/EMCEurope.2019.8871728.

[32] J. Luo, E. Mendivil, and M. Christopher, "Obtaining total isotropic sensitivity from average fading sensitivity in reverberation chamber," in *Proc. 2017 IEEE Int. Symp. Antennas Propag. USNC/URSI Nat. Radio Sci. Meeting*, pp. 241–242, doi: 10.1109/APUSNCURSINRSM.2017.8072163.

[33] B. L. Goldstein and K. A. Remley, "Next-generation IIoT: A convergence of technology revolutions," *Nat. Acad. Eng. Bridge*, vol. 51, no. 1, pp. 33–40, Apr. 2021.

[34] D. Senic *et al.*, "Estimating and reducing uncertainty in reverberation-chamber characterization at millimeter-wave frequencies," *IEEE Trans. Antennas Propag.*, vol. 64, no. 7, pp. 3130–3140, 2016, doi: 10.1109/TAP.2016.2556711.

[35] A. K. Fall, P. Besnier, C. Lemoine, M. Zhadobov, and R. Sauleau, "Design and experimental validation of a mode-stirred reverberation chamber at millimeter waves," *IEEE Trans. Electromagn. Compat.*, vol. 57, no. 1, pp. 12–21, 2015, doi: 10.1109/TEMC.2014.2356712.

[36] A. Hubrechsen, A. C. F. Reniers, A. B. Smolders, and L. A. Bronckers, "Chamber-decay time in a mm-wave reverberation chamber," in *Proc. 2021 IEEE Int. Symp. Antennas Propag. USNC-URSI Radio Sci. Meeting*, submitted for publication.

[37] A. Hubrechsen, S. J. Verwer, A. C. F. Reniers, L. A. Bronckers, and A. B. Smolders, "Pushing the boundaries of antenna-efficiency measurements towards 6G using a novel mm-wave reverberation chamber," in *Proc. 2021 IEEE Conf. Antenna Meas. Appl.* (CAMA 2021), Antibes Juan-les-Pins, France, pp. 263–265.